Turbo-DC-FPSK: a joint turbo coding and FPSK based modulation scheme adapted to optical wireless communications

Paul Miqueu, Muhammad Jehangir Khan, Yannis Le Guennec, Laurent Ros

Turbo-DC-FPSK: a joint turbo coding and FPSK based modulation scheme adapted to optical wireless communications.

1st Miqueu Paul
Gipsa-lab
Saint Martin d'Hères, France
paul.miqueu@grenoble-inp.fr

2nd Khan Muhammad Jehangir
Gipsa-lab
Saint Martin d'Hères, France
muhammad-jehangir.khan@grenoble-inp.fr

3rd Le Guennec Yannis
Gipsa-lab
Saint Martin d'Hères, France
yannis.le-guennec@grenoble-inp.fr

4th Ros Laurent
Gipsa-lab
Saint Martin d'Hères, France
laurent.ros@grenoble-inp.fr

***Abstract*—This letter proposes and analyzes a flexible and energy efficient technique for Optical Wireless Communication (OWC) systems. It involves the Direct Current - Frequency and Phase Shift Keying (DC-FPSK) modulation combined with a very low complexity convolutional code in a parallel scheme at the transmitter side, and a turbo-decoder at the receiver side, i.e. Bahl, Cocke, Jelinek and Raviv (BCJR) algorithm. It is an adaptation of the coplanar turbo-FSK technique developed for the long range low power Radio-Frequency (RF) context to the OWC requirements, to be compatible with Intensity-Modulation Direct Detection (IM-DD) techniques (real positive base-band waveforms including a Direct Current (DC) component instead of complex waveforms). Simulation results show that turbo-DC-FPSK can achieve around 5 dB energy gain over regular OWC state-of-the-art DC-FPSK modulation at a BER $= 10^{-4}$. Using the number of linear modulation states as degrees of freedom, a flexibility in the desired balance between energy efficiency and spectral efficiency is achieved.**

***Index Terms*—Frequency and Phase Shift Keying (FPSK), Intensity Modulation and Direct Detection (IM-DD), Optical Wireless Communication (OWC), turbo coding, Discrete Fourier Transform (DFT).**

I. Introduction

OPTICAL Wireless Communication (OWC) systems are developed to be used in parallel with the traditional Radio Frequency (RF) systems for applications such as vehicle-to-vehicle communications [1] and biomedical sensing data networks [2] that require transmission of sporadic small amount of data with low data rate. In a low complexity OWC system, Intensity-Modulation Direct Detection (IM-DD) technique is used: data is transmitted by modulating the intensity of a Light Emitting Diode (LED) and recovered, after wireless transmission, by a photodiode [3]. The requirements for IM-DD are different than for RF systems since there is no phase/quadrature modulation of a carrier frequency, and light intensity shows only real and positive values. It restricts the use to a real and positive baseband signal, whereas RF systems can use complex and bipolar waveforms in the baseband domain (before carrier frequency shift).

A large number of linear modulations have been investigated for high data rate OWC applications, such as M-ary Pulse Amplitude Modulation (M-PAM) [4], or Orthogonal Frequency Division Multiplexing (OFDM) [5] due to their high spectral efficiency. Yet, because OWC can be affected by strong path loss, it is relevant to investigate specific high energy efficiency modulation schemes in the context of low data rate communications. In [6], A. W. Azim & al. proposed an energy efficient Direct-Current - Frequency Shift Keying (DC-FSK) modulation technique with reduced spectral efficiency (i.e. compatible with low data rate communications) and dealing with IM-DD constraints of OWC systems. M-ary DC-FSK modulation scheme takes advantage of the orthogonal nature of the FSK modulation to reach high energy efficiency when increasing modulation order M, unlike linear modulation. Additionally, M-ary DC-FSK modulation benefits from constant envelop, which lowers the impact of LED non-linearity [7], reduces the flickering effect and exhibits natural robustness against frequency selective channels [6]. Yet, high energy efficiency is achieved at the expense of spectral efficiency reduction. In order to compensate for the weak spectral efficiency induced by DC-FSK signaling, a linear Phase Shift Keying (PSK) modulation method has been combined to DC-FSK to define DC-FPSK modulation scheme in [8]. Addition of M_ϕ phases to the $M_\perp$ DC-FSK orthogonal[1] symbols increases the modulation order ($M = M_\phi M_\perp$) while maintaining the waveforms' bandwidth constant, leading to an increase of $(M_\perp, M_\phi)$-DC-FPSK spectral efficiency relatively to DC-FSK. It has been shown in [8] that, for a moderate value of M_ϕ = 4, DC-FPSK's spectral efficiency is 4 times

[1]In this article, DC-FPSK symbols are loosely described as "orthogonal" since the inner product between two different symbols is not zero but is equal to the squared of the DC value

higher than DC-FSK's, while maintaining an identical energy efficiency.

In radio applications, it is widely known that turbo-coding methods can drastically improve communication system's energy efficiency [9]. Recently, optimized joint turbo coding with FSK or FPSK modulation (respectively called turbo-FSK [10], and coplanar turbo-FSK [11]) have been developed for the long range low power RF context as well as for the Internet-of-Things (IoT) context. In [11], the technique renamed here turbo-FPSK combines energy efficient $(M_{\perp}, M_{\phi})$-FPSK modulation with a very low complexity convolutional code in a parallel concatenated scheme at the transceiver and uses a joint turbo decoder at the receiver. It has been demonstrated in [11] that turbo-FPSK achieves very low levels of required energy per bit, while ensuring a low complexity transmitter and a constant envelope modulation scheme. However, as these turbo-processing schemes have been designed to fit the RF context, they can not be directly applied to IM-DD OWC systems. In [12], turbo coding has been investigated for On-Off-Keying (OOK) OWC systems, but OOK is sensitive to frequency selective OWC channels and, as a linear modulation, it is not as energy efficient as orthogonal modulation scheme. In [13], a turbo coded OFDM modulation scheme adapted to OWC constraints is proposed for high data rate applications, but still suffers from limited energy efficiency due to the use of a linear modulation and due to OFDM high Peak to Average Power Ratio (PAPR).

In this paper, for the first time to the authors' knowledge, an adaptation of (carrier based RF) turbo-FPSK for low data rate, energy efficient OWC systems is proposed. More particularly, joint turbo processing and DC-FPSK modulation/demodulation method is proposed. The resulting proposed turbo-DC-FPSK scheme can be regarded as an extension of two low data rate OWC state-of-the-art schemes that we have previously proposed (namely the original DC-FSK scheme [8], extended now by joint modulation coding and turbo process, and the original turbo-DC-FSK scheme [14], extended now by the concept of hybrid modulation through the additional PSK modulation). The new spectral efficiency derivation and turbo-DC-FPSK OWC system performances are provided and discussed. A strong energy gain (respect. spectral efficiency increase) is achieved for a given spectral efficiency (respect. a given energy efficiency) when compared to the OWC state-of-the-art scheme DC-FPSK (respect. turbo-DC-FSK)

The rest of the paper is organized as follows. The proposed turbo-DC-FPSK technique is presented in section II, followed by simulation results and performance discussion in section III. Finally conclusion is presented in section IV.

II. Proposed turbo FPSK in the OWC context

A. Transceiver overview

a) Turbo Encoder: Fig. 1 shows the scheme of the turbo DC-FPSK transceiver. It receives a binary word made out of n bits. Following the scheme of a standard turbo encoder, words are copied λ times and sent on parallel branches. Each branch has its own interleaving pattern. On each branch, words are

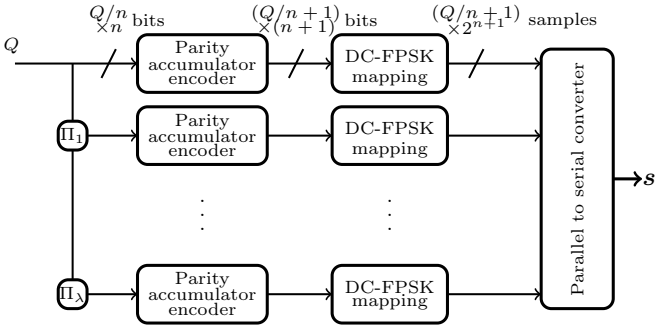

Fig. 1. Turbo-DC-FPSK transmitter architecture with joint turbo encoder/DC-FPSK modulator

encoded by a parity accumulator encoder that adds only one bit to each word to limit the system's complexity. The form of the convolutional encoder is due to the BCJR algorithm at the receiver that combines decoding with demodulation when using a parity accumulator encoder at the transmitter. This bit is the sum modulus 2 between the parity of the word and the value that was saved in the memory slot of the encoder. The memory slot's value is updated with the value of the added bit. This encoder is a convolutional encoder as the parity bit of each information word is computed. We further detail the time invariant trellis associated to it in the following paragraph.

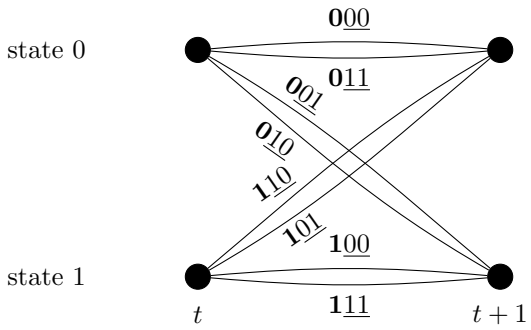

Fig. 2. Parity accumulator encoder trellis for $n = 2$

b) FPSK Mapping: The parity accumulator encoder has two states as its memory slot can take two values, 1 or 0, and the transition between states is ruled by the input codeword parity. Either the input codeword has a even parity and the state remains the same, either it has an odd parity and the state changes. The trellis that illustrates this behavior is displayed on Fig. 2 for words made out of $n = 2$ information bits. On Fig. 2, we consider the transitions between two dates of indexes t and $t + 1$, input information bits are underlined while the added bit is in bold case. After the parity accumulator encoder there are $M = 2^{n+1} = 8$ codewords.

The trellis is used at the receiver side to determine the group of codewords the most likely to have been sent between the sampling dates of indexes t and $t + 1$, knowing a particular transition in the memory slot state occurred between t and $t + 1$.

Finally, there exist various mapping patterns of the waveforms on the codewords. Considering how the waveforms are mapped to the trellis, and thus, are mapped to the codewords, the performance of the system fluctuates according to [11]. We introduce the waveforms dictionary we use in this system before further detailing its mapping.

c) Alphabet Generation: The FPSK alphabet is made out of M waveforms divided into $M_\perp$ orthogonal subsets. Each subset contains M_ϕ phase shifts of the initial waveform, as illustrated in Fig. 3. Waveforms are, thus, orthogonal with waveforms coming from the other subsets. We decompose a codeword made out of $n+1$ bits into $n+1 = n_\phi + n_\perp + 1$. It gives the modulation order $M = 2^{n+1} = M_\phi M_\perp$ with $M_\phi = 2^{n_\phi}$ and $M_\perp = 2^{n_\perp+1}$.

In time-domain, waveforms are real pure tone (cosinus type) signals with frequencies spaced by Δf (as basis of the orthogonal subset), completed by additional phase shifts (for the linear modulation part).

In the frequency domain, a waveform is then defined by its positive discrete frequency $f_m = m\Delta f$, with $m \in [1, M_\perp]$ (m is the frequency index), and its (linear modulation) complex amplitude:

$$z_i = \exp\{j2\pi i/M_\phi\} \tag{1}$$

with $i \in [0, M_\phi - 1]$ being the phase shift index and $j^2 = -1$, the imaginary coefficient. The spectrum of the waveform can be described by a frequency vector $\boldsymbol{F}_{m,i}$, with all components equal to zero, except for the two ones corresponding to frequencies f_m and $-f_m$, due to the Hermitian symmetry, as we deal with real time domain waveforms. To be compatible with Discrete Fourier Transform (DFT) and inverse DFT (iDFT) operations, this vector contains first positive and then negative frequency components, such that:

$$\boldsymbol{F_{m,i}} = [\overset{DC}{\downarrow}\ 0\ , \underbrace{0, \cdots, 0, \overset{m+1\text{-th sample}}{\downarrow}\ \bar{z}_i\ , 0, \cdots, 0,}_{M_\perp \text{ samples}} \underbrace{0, \cdots, 0, \overset{2M_\perp - m + 2\text{-th sample}}{\downarrow}\ \bar{z}_i\ , 0, \cdots, 0}_{M_\perp \text{ samples}}]^T, \tag{2}$$

where overline denotes the conjugate. Note that we do not consider the waveform for index $m = 0$ in our dictionary as it cannot be phase modulated. We get a frequency vector of size $2M_\perp + 1$, which corresponds to the minimum number of chips M_c required to represent the waveforms in time-domain according to [8]. In this work, the number of chips is fixed to the minimum required, $M_c = 2M_\perp + 1$. It should be noted that unlike our previous work dealing with turbo-DC-FSK (without phase shifts) [14], the proposition in this paper is based on DFT instead of Discrete Cosine Transform (DCT) to ease the processing related to the additional phase shifts.

The sampled waveform in the time domain is a M_c samples vector $\tilde{\mathbf{c}}_{m,i}$ that can be computed by a M_c order iDFT applied on $\boldsymbol{F}_{m,i}$ as follows:

$$\tilde{\boldsymbol{c}}_{m,i} = \text{iDFT}_{M_c}\{\boldsymbol{F}_{m,i}\} \tag{3}$$

Consequently, the k-th component of $\tilde{\boldsymbol{c}}_{m,i}$ with $k \in \{0, ..., M_c - 1\}$, is expressed as:

$$\begin{aligned} \tilde{\mathbf{c}}_{m,i}(k) &= \cos\left(2\pi f_m k T_c + \phi_i\right) \\ &= \Re(z_i.\tilde{\mathbf{s}}_m(k)) \end{aligned} \tag{4}$$

It is the real part of the multiplication (with $\Re(.)$ the real operator) between the complex pure frequency waveform:

$$\tilde{s}_m(k) = \exp\{j2\pi f_m k T_c\} \tag{5}$$

and the complex phase shift z_i expressed in Eq. (1). T_c is the sampling period such that $T_c = T_s/M_c$ with T_s the total duration of the waveform.

The required orthogonal condition between the $M_\perp$ complex waveforms $\tilde{s}_m(k)$ gives $\Delta f = 1/T_s$ (whereas the orthogonal condition was $\Delta f = 1/2T_s$ in [14] as we were only considering real waveforms without phase shift). The single sided bandwidth B of the transmitted baseband signal is then :

$$\begin{aligned} B &= M_\perp \Delta f = M_\perp \frac{1}{T_s} \\ B &= \frac{M_\perp}{(2M_\perp + 1)T_c} \end{aligned} \tag{6}$$

We notice that for large alphabet size, $B \approx \frac{1}{2T_c}$, which agrees with the Shannon-Nyquist sampling theorem.

Now that we have defined the FPSK dictionary we use, we focus on the mapping of the dictionary waveforms to the binary codewords because according to [11], the performance of the system depends on the FPSK waveforms' mapping. We chose the X-mapping for our trellis as it shows the best results according to [11] and is easy to implement: lightest bits of the binary codeword encode for the frequency index while the heaviest ones encode for the phase shift index. The X-mapping of the binary codewords to the waveforms of the dictionary is illustrated on Fig. 3 while the mapping of the waveforms into the trellis is displayed on Fig. 4 for $M = 8 = 2^{2+1}$.

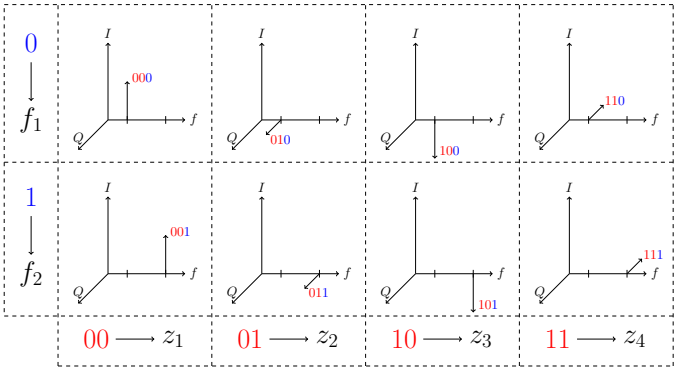

Fig. 3. (2,4)-FPSK mapping scheme for a X-mapping

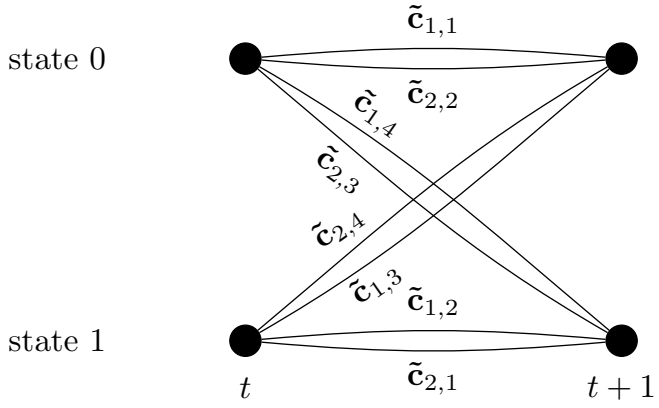

Fig. 4. Trellis X-mapping associated to a (2,4)-FPSK mapping.

To make the waveforms unipolar and positive, a DC component is added to the FPSK waveforms issued from the iDFT, to define the DC-FPSK waveforms. The amplitude A of the DC-FPSK waveforms is also introduced as parameter. As the cosine function ranges from -1 to 1, the minimum required DC component is A, resulting in a range from 0 to $2A$ for the DC-FPSK waveform amplitude. The DC-FPSK waveform, $\mathbf{c}_{m,i}$ corresponding to the m-th frequency and i-th phase is then expressed as:

$$\boldsymbol{c}_{m,i} = A\ \tilde{\mathbf{c}}_{m,i} + A = A\ \text{iDFT}_{2M_\perp+1}\{\boldsymbol{F}_{m,i}\} + A \quad (7)$$

Adding this DC component degrades the energy efficiency of the system. We compare the electrical symbol energy E_s of a unipolar and a bipolar FPSK waveform:

$$E_{\mathbf{s}} = \begin{cases} (\frac{A^2}{2} + A^2)T_s & \text{for DC-FPSK unipolar waveforms,} \\ \frac{A^2}{2}T_s & \text{for bipolar FPSK waveforms.} \end{cases} \quad (8)$$

An increase of $10 \times log_{10}(3) \approx 5$ dB is induced on DC-FPSK symbol energy relatively to FPSK symbol due the DC bias addition (for the same thermal noise robustness).

To fully scale the performance of our communication system, we consider its spectral efficiency η. It is defined as $\eta = R/B$ with R the data rate (in bit/s) of the system and B (in Hz) its bandwidth. Considering the number of samples per waveform $M_c = 2M_\perp + 1$ and an information block of Q bits, we have:

$$R = \frac{Q}{\lambda(\frac{Q}{n}+1)(2M_\perp+1)T_c} \quad (9)$$

We remind that $n+1 = \log_2(M)$, thus, $n = \log_2(M) - 1$. It gives:

$$\eta = \frac{Q}{\lambda(\frac{Q}{\log_2(M)-1}+1)M} M_\phi \quad (10)$$

For a large information block (Q large), $\eta \approx \frac{log_2(M)-1}{\lambda M} M_\phi$. The impact of the convolutional encoding step on the spectral efficiency of the system fades away. We get the spectral efficiency of a regular FPSK modulation method with a repetition of λ times the information to transmit.

Given the spectral efficiency expression, we understand that increasing the number of linear modulation states increases the spectral efficiency. There are three degrees of freedom in Eq. 10:

- M, the overall alphabet size.
- M_ϕ, the number of linear modulation states.
- λ, the number of parallel branches.

B. Receiver overview

a) Additive White Gaussian Noise (AWGN) Channel: We assume that the signal is transmitted over an AWGN channel. The observation model follows:

$$\boldsymbol{r} = \boldsymbol{c} + \boldsymbol{w}, \quad (11)$$

with $\boldsymbol{c}$ a waveform issued from the M-ary DC-FPSK alphabet and $\boldsymbol{r}$ the noisy received waveform. The AWGN vector $\boldsymbol{w}$ has a single-sided power spectral density N_0. The components of $\boldsymbol{w}$ are independent, each following a centered gaussian law $N(0;\sigma^2)$, with a mean power $\sigma^2 = N_0 B$.

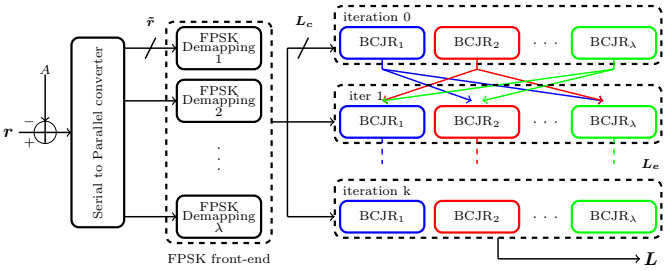

Fig. 5. Turbo-DC-FPSK receiver

b) Combined Demodulation and Decoding: The receiver is represented on Fig. 5. It is built according to the turbo process structure.

We briefly recall that the turbo process is iterative and aims at computing for each information bit its Log Likelihood Ratio (LLR). Either the LLR is positive and the bit is likely to be a

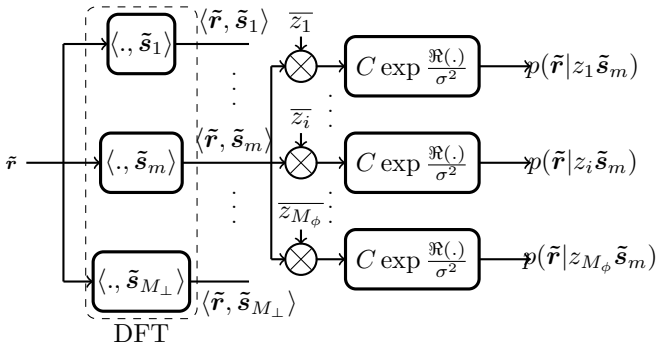

Fig. 6. Detail of the soft FPSK demapper for one of the parallel branches.

1, either the LLR is negative and the bit is likely to be a 0. The process is illustrated on the right hand side of the Fig. 5. For a given branch of index l (with $l \in [\![1, \lambda]\!]$), at iteration step j (with $j \in [\![1, \nu]\!]$), the computation of the information bit LLR relies on the channel observations and the extrinsic information coming from the $\lambda - 1$ branches (all the branches except the one of index i) computed during the previous iteration step of index $j - 1$ (except for the first iteration step that relies on channel observations only).

Channel observations, after having been centered by subtracting the DC component A, $\tilde{r} = r - A$, provide, for each branch, for each symbol period, all the FPSK dictionary codewords' likelihoods. Likelihoods are computed according to Fig. 6 for one out of the λ parallel branches. It relies on the correlation between the channel observations and the dictionary waveforms for each symbol period. It should be noted that the $M = M_\perp M_\phi$ inner products $\langle \tilde{\boldsymbol{r}}, \tilde{\boldsymbol{c}}_{m,i} \rangle = \langle \tilde{\boldsymbol{r}}, \Re(z_i \tilde{\boldsymbol{s}}_m) \rangle$ can be replaced by $\Re(\langle \tilde{\boldsymbol{r}}, \tilde{\boldsymbol{s}}_m \rangle \bar{z}_i)$. These correlations can be computed by a single DFT of size $M_c = 2M_\perp + 1$ of the channel observations. The DFT coefficients (i.e. $\langle \tilde{\boldsymbol{r}}, \tilde{\boldsymbol{s}}_m \rangle$) are then multiplied by $\bar{z}_i$ and used to compute the codewords likelihoods. The likelihoods for each symbol period, each codeword and each branch are stacked into the $\boldsymbol{L_c}$ matrix which has a size $\lambda \times \frac{Q}{n} \times M$. It is the same matrix that is provided to every iteration step. More details on the codewords' likelihood can be found in [8], [10], [11], [14].

Extrinsic information comes from the information bits' LLRs output by the BCJR algorithms of the previous iteration step. Indeed, in our application, the information bit LLR is computed thanks to the BCJR algorithm as we are using a parity accumulator encoder at the transceiver. It combines decoding with demodulation as the receiver has not the standard form consisting of a demodulator followed by a decoder. We remind that, at the transmission side, neighboring symbols are linked by the parity accumulator encoder and share information. Indeed, knowing the transition that occurred between two dates, a group of codewords is more likely to have been sent and that is the information the BCJR algorithm uses. The probability of a transition to occur is computed according to the channel observations and extrinsic information output by the previous iteration step. Eventually, the extrinsic information (the information created by the BCJR algorithm) is the difference between the LLR computed by the BCJR algorithm and the a priori probability of each information bit. It is arranged in a vector of size $Q/n \times M$ noted $\boldsymbol{L_e}$ on Fig. 5 and is then sent to other branches' BCJR algorithms to proceed to the next iteration step.

At the end of the turbo process the information bits' LLRs output by the BCJR algorithms of the last iteration step are arranged in the $\boldsymbol{L}$ vector of size Q.

Simulation results will give an idea of the performance of the communication system in a theoretical environment.

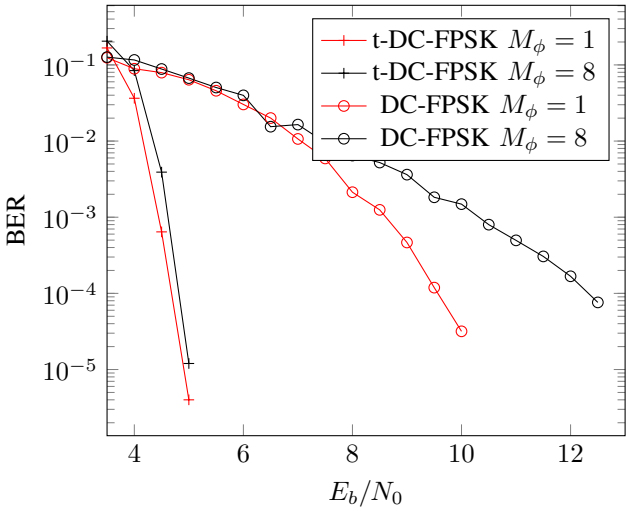

Fig. 7. BER vs required E_b/N_0 performance comparison between turbo-DC-FPSK and DC-FPSK for the same alphabet size $M = 128$ but different number of phases $M_\phi \in \{1, 8\}$. $\lambda = 4$, $Q = 1024$ and $\nu = 10$. We outline that spectral efficiencies are different for every method.

III. Simulation Results

A. BER Performances over AWGN Channel

Fig. 7 shows simulated BER as a function of E_b/N_0 for DC-FPSK and turbo-DC-FPSK, considering $M_\phi \in \{1; 8\}$ and a fixed overall alphabet size $M = M_\perp M_\phi = 128$. The turbo process goes through $\nu = 10$ iterations and the number of branches is $\lambda = 4$. We chose these particular alphabet size M and number of parallel branches as these values are the ones for which the turbo-DC-FSK is expected to reach the best energy efficiency according to [10]. We first notice the performance improvement brought by the coding step. Considering turbo-(128,1)-DC-FPSK and (128,1)-DC-FPSK the energy efficiency gap is about 5 dB for a BER of 10^{-4}. We also notice that adding phases to the FSK alphabet lowers the energy efficiency (i.e. it requires a higher E_b/N_0 to reach a given BER) of the system. It is a foreseen result as the BCJR algorithm performance relies on the orthogonality of the modulation alphabet (which is globaly lost after adding the phase shifts). Nevertheless, these four methods present different spectral efficiencies. Adding a coding step and a turbo process highly improves the performance of the system considering the energy efficiency, but it also degrades its spectral efficiency significantly. To quantify the overall turbo-coded modulation efficiency, we thus need to investigate the evolution of spectral efficiency versus energy efficiency, which is the aim of the next section.

B. Spectral Efficiency versus Energy Efficiency

Fig. 8 shows the evolution of spectral efficiency as a function of the required E_b/N_0 to reach a target BER of 10^{-4} for different orthogonal alphabet sizes $M_\perp$, and phase modulation alphabet sizes M_ϕ, assuming a fixed overall alphabet size $M = M_\phi M_\perp = 128$ and a number of branches of $\lambda = 4$. The turbo process goes through $\nu = 10$ iterations.

We notice on Fig. 8 that the energy efficiency of the turbo-DC-FPSK system is the same for $n_\phi \in [\![1, n_\phi^{min}]\!]$ with $M_\phi^{min} = 2^{n_\phi^{min}} = 8$, while its spectral efficiency is improving with M_ϕ. We notice that the spectral efficiency improves from 3×10^{-3} bits/s/Hz (for $M_\phi = 1$) to 5×10^{-2} bits/s/Hz (for $M_\phi = 8$) which is a spectral efficiency gain factor of approximately 20. Considering [11] and simulations we ran for smaller alphabet sizes, this behavior (existence of a M_ϕ^{min}) extends to all alphabet size M when considering the turbo-DC-FPSK.

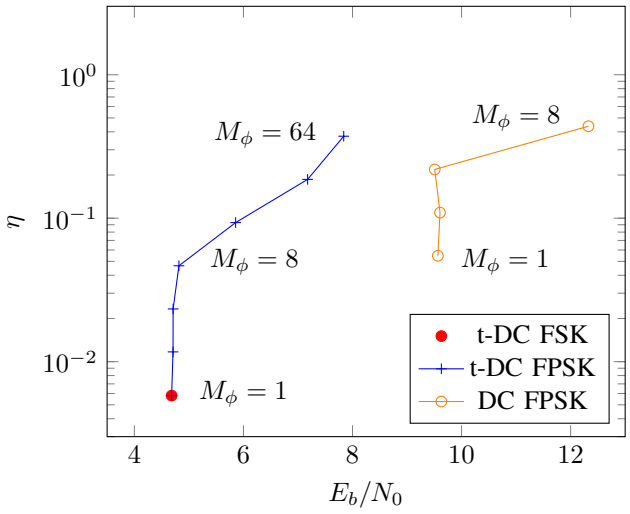

Fig. 8. Spectral efficiencies of turbo-DC-FPSK (t-DC-FPSK) as a function of the required E_b/N_0 to reach a BER of 10^{-4}, for a given alphabet size of $M = 128$ but different number of linear modulation states $M_\phi = 2^{n_\phi}$ with $n_\phi \in [\![1, 6]\!]$ for the turbo-DC-FPSK and $n_\phi \in [\![1, 3]\!]$ for the regular DC-FPSK. For the turbo process $Q = 1024$, $\lambda = 4$ and $\nu = 10$.

It makes obsolete the use of turbo-DC-FPSK system with less than M_ϕ^{min} linear modulation states, especially the turbo-DC-FSK ($M_\phi = 1$) [14]. Adding more than M_ϕ^{min} modulation states can be useful if the system requires a specifically high spectral efficiency, but the best parameters are to be worked out considering the energy/spectral efficiency trade off. Finally, we compare in Fig. 8 turbo-DC-FSPK and DC-FPSK. Although, we notice the degradation in spectral efficiency brought by turbo coding, we also notice that linear modulation enables us to fill this gap.

Indeed, the turbo-(16,8)-DC-FSPK method reaches the same spectral efficiency as the DC-FSK method while safekeeping the energy efficiency improvement of nearly 5 dB brought by the turbo coding step.

To be complete, it has to be noted that the larger is the information block (the larger is Q), the better the system works according to [10] where performances are given for $Q \in \{100, 1000, 100000\}$. Also, the turbo coding step highly increases the system's complexity. The BCJR algorithm requires numerous computations depending on the alphabet size and the size of the bit sequence. Turbo-DC-FSK is more relevant for up-link transmission scenarios between a sensor and an access point, for which the increase of complexity and related power consumption will be mainly assumed in the access point, while the complexity overhead in the sensor will be limited.

IV. Conclusion

We adapted the turbo-FPSK method (initially developed for long range low power RF context) to the Intensity Modulation/Direct Detection (IM/DD) constraints of OWC. The resulting turbo-DC-FPSK proposed scheme can also be regarded as an extension of the DC-FPSK modulation scheme (belonging to OWC state of the art). The extension consists of a mix of coding and modulation at transmitter, implying the use of a turbo decoder at the receiver.

- First, the proposed turbo-DC-FPSK scheme demonstrated significant performance improvement compared to the DC-FPSK modulation method. Indeed, for a given spectral efficiency in the expected application range (10^{-1} to 10^{-2} bit/sec/Hz), turbo-DC-FPSK can achieve around 5 dB energy gain over regular DC-FPSK for a target BER = 10^{-4}. These results are enable by an increase in the system's complexity but it can be a relevant choice for up-link transmission scenarios between sensors and an access point.
- Secondly, we highlighted the relevancy of adding linear modulation states ($i.e.$ phase shifts) to a regular turbo-DC-FSK system for a given alphabet size M. It enables to greatly improve the spectral efficiency of the system without lowering its energy efficiency when adding up to M_ϕ^{min} linear modulation states for any alphabet size.

References

[1] K. Siddiqi, A. D. Raza, and S. S. Muhammad, "Visible light communication for V2V intelligent transport system," in *2016 International Conference on Broadband Communications for Next Generation Networks and Multimedia Applications (CoBCom)*, pp. 1–4, 2016.

[2] Y.-K. Cheong, X.-W. Ng, and W.-Y. Chung, "Hazardless biomedical sensing data transmission using VLC," *IEEE Sensors Journal*, vol. 13, no. 9, pp. 3347–3348, 2013.

[3] H. Haas, L. Yin, Y. Wang, and C. Chen, "What is LiFi?," *Journal of lightwave technology*, vol. 34, no. 6, pp. 1533–1544, 2015.

[4] A. Nuwanpriya, S.-W. Ho, J. A. Zhang, A. J. Grant, and L. Luo, "PAM-SCFDE for optical wireless communications," *Journal of Lightwave Technology*, vol. 33, no. 14, pp. 2938–2949, 2015.

[5] S. D. Dissanayake and J. Armstrong, "Comparison of ACO-OFDM, DCO-OFDM and ADO-OFDM in IM/DD systems," *Journal of lightwave technology*, vol. 31, no. 7, pp. 1063–1072, 2013.

[6] A. W. Azim, A. Rullier, Y. Le Guennec, L. Ros, and G. Maury, "Energy efficient M-ary frequency-shift keying-based modulation techniques for visible light communication," *IEEE Transactions on Cognitive Communications and Networking*, vol. 5, no. 4, pp. 1244–1256, 2019.

[7] I. Stefan, H. Elgala, and H. Haas, "Study of dimming and LED nonlinearity for ACO-OFDM based VLC systems," in *2012 IEEE Wireless Communications and Networking Conference (WCNC)*, pp. 990–994, 2012.

[8] A. W. Azim, Y. Le Guennec, and L. Ros, "Hybrid frequency and phase-shift keying modulation for energy efficient optical wireless systems," *IEEE wireless communications letters*, vol. 9, no. 4, pp. 429–432, 2019.

[9] L. Ping, W. Leung, and K. Y. Wu, "Low-rate Turbo-Hadamard codes," *IEEE Transactions on Information Theory*, vol. 49, no. 12, pp. 3213–3224, 2003.

[10] Y. Roth, J.-B. Doré, L. Ros, and V. Berg, "Turbo-fsk, a physical layer for low-power wide-area networks: Analysis and optimization," *Comptes Rendus Physique*, vol. 18, no. 2, pp. 178–188, 2017.

[11] Y. Roth, J.-B. Doré, L. Ros, and V. Berg, "Coplanar turbo-FSK: A flexible and power efficient modulation for the internet-of-things," *Wireless Communications and Mobile Computing*, vol. 2018, 2018.

[12] S. H. Lee and J. K. Kwon, "Turbo code-based error correction scheme for dimmable visible light communication systems," *IEEE Photon. Technol. Lett.*, vol. 24, no. 17, pp. 1463–1465, 2012.

[13] M. Ataee, M. S. Sadough, and Z. Ghassemlooy, "An adaptive Turbo coded-OFDM scheme for visible light communications," in *2019 2nd West Asian Colloquium on Optical Wireless Communications (WACOWC)*, pp. 1–5, 2019.

[14] P. Miqueu, M. J. Khan, Y. Le Guennec, and L. Ros, "Turbo-dc-fsk: Joint turbo coding and fsk-based modulation for visible light communications," in *2022 Joint European Conference on Networks and Communications & 6G Summit (EuCNC/6G Summit)*, pp. 25–30, IEEE, 2022.